

# Addressing controversies in the xylem embolism resistance–vessel diameter relationship

Emilie Isasa<sup>1\*</sup> , Roman Mathias Link<sup>1,2\*</sup> , Steven Jansen<sup>3</sup> , Fon Robinson Tezeh<sup>1</sup> , Lucian Kaack<sup>3</sup> ,  
Juliano Sarmiento Cabral<sup>4,5†</sup>  and Bernhard Schuldt<sup>1,2†</sup> 

<sup>1</sup>Ecophysiology and Vegetation Ecology, Julius-von-Sachs-Institute of Biological Sciences, University of Würzburg, Julius-von-Sachs-Platz 3, 97082 Würzburg, Germany; <sup>2</sup>Chair of Forest Botany, Institute of Forest Botany and Forest Zoology, Technical University of Dresden, Piennner Str. 7, 01737 Tharandt, Germany; <sup>3</sup>Institute of Systematic Botany and Ecology, Ulm University, Albert-Einstein-Allee 11, 89081 Ulm, Germany; <sup>4</sup>Ecosystem Modeling Group, Center for Computational and Theoretical Biology, University of Würzburg, Klara-Oppenhaimer-Weg 32, 97074 Würzburg, Germany; <sup>5</sup>Biodiversity Modelling and Environmental Change, School of Biosciences, College of Life and Environmental Sciences, University of Birmingham, Birmingham, B15 2TT, UK

Author for correspondence:  
Roman Mathias Link  
Email: [roman.link@plant-ecology.de](mailto:roman.link@plant-ecology.de)

Received: 14 July 2022  
Accepted: 6 December 2022

New Phytologist (2023) **238**: 283–296  
doi: 10.1111/nph.18731

**Key words:** angiosperm xylem, data aggregation, embolism resistance, functional traits, hydraulic conductivity, pit membrane, vessel diameter.

## Summary

- Although xylem embolism is a key process during drought-induced tree mortality, its relationship to wood anatomy remains debated. While the functional link between bordered pits and embolism resistance is known, there is no direct, mechanistic explanation for the traditional assumption that wider vessels are more vulnerable than narrow ones.
- We used data from 20 temperate broad-leaved tree species to study the inter- and intraspecific relationship of water potential at 50% loss of conductivity ( $P_{50}$ ) with hydraulically weighted vessel diameter ( $D_h$ ) and tested its link to pit membrane thickness ( $T_{PM}$ ) and specific conductivity ( $K_s$ ) on species level.
- Embolism-resistant species had thick pit membranes and narrow vessels. While  $D_h$  was weakly associated with  $T_{PM}$ , the  $P_{50}$ – $D_h$  relationship remained highly significant after accounting for  $T_{PM}$ . The interspecific pattern between  $P_{50}$  and  $D_h$  was mirrored by a link between  $P_{50}$  and  $K_s$ , but there was no evidence for an intraspecific relationship.
- Our results provide robust evidence for an interspecific  $P_{50}$ – $D_h$  relationship across our species. As a potential cause for the inconsistencies in published  $P_{50}$ – $D_h$  relationships, our analysis suggests differences in the range of trait values covered, and the level of data aggregation (species, tree or sample level) studied.

## Introduction

Xylem embolism formation, that is the disruption of water flow by the formation of large gas bubbles in xylem conduits, is a key process contributing to drought-induced tree mortality (Anderegg *et al.*, 2016; Adams *et al.*, 2017; Powers *et al.*, 2020; Arend *et al.*, 2021; Hajek *et al.*, 2022). Therefore, recent work has been focused on analysing the mechanisms that are at play during embolism formation, and on identifying xylem functional traits that are associated with embolism risk (Lens *et al.*, 2022).

While the role of xylem embolism in mortality under drought is widely accepted, the exact mechanistic processes involved in embolism formation remain not well known. Along the hydraulic pathway from roots to leaves, the water column inside the xylem is under negative pressure and hence in a metastable state (Tyree & Zimmermann, 2002). As the water potentials necessary for a spontaneous transition from the liquid to the gas phase (i.e. homogeneous cavitation) exceed water potentials observed in living plants

by orders of magnitude (Herbert & Caupin, 2005; Stroock *et al.*, 2014; Kanduč *et al.*, 2020), this process is unlikely to substantially contribute to embolism formation. The prevailing assumption is hence that embolism formation is triggered by ‘air seeding’, that is when gas bubbles enter functional conduits through the pores of pit membranes that are connected to adjacent, embolized conduits (Sperry & Tyree, 1988; Brodersen *et al.*, 2013; Jansen *et al.*, 2018; Roth-Nebelsick, 2019). Pit membranes hereby play the role of safety valves that prevent embolism from spreading to neighbouring vessels (Meyra *et al.*, 2007; Choat *et al.*, 2008). Because pit membranes provide the largest pores and highest permeability between adjacent vessels, their structure is directly linked to embolism resistance (Wheeler *et al.*, 2005; Jansen *et al.*, 2009). More specifically, pit membrane thickness ( $T_{PM}$ ) has been singled out as a key determinant of embolism resistance due to its direct relation to the size distribution of pore constrictions in pit membranes (Li *et al.*, 2016; Bai *et al.*, 2020; Kaack *et al.*, 2021).

How embolism propagation at the pit membrane level translates to larger-scale wood anatomical features, particularly to vessel dimensions, is subject to current debate (Kaack *et al.*, 2021; Lemaire *et al.*, 2021; Levionnois *et al.*, 2021). Here, a long-

\*These authors shared first authorship.

†These authors shared senior authorship.

standing assumption is that vessel diameter is negatively related to resistance against drought-induced embolism, which is thought to form the basis for an apparent trade-off between embolism safety and hydraulic efficiency (Tyree *et al.*, 1994; Tyree & Zimmermann, 2002; Wheeler *et al.*, 2005). However, there is no known mechanism that constitutes a direct link between vessel size and embolism resistance (Anfodillo & Olson, 2021), while the evidence for a stability-efficiency trade-off is frequently weak (Gleason *et al.*, 2016).

In general, there is substantial controversy regarding the impact of vessel diameter on drought-induced embolism (Lens *et al.*, 2022), and the existing evidence for a relationship is inconsistent (Anfodillo & Olson, 2021). In studies focusing on interspecific patterns, it is often found that vessel diameter is positively associated with the water potential at 50% loss of hydraulic conductivity ( $P_{50}$ ; Hacke *et al.*, 2006, 2017; Maherali *et al.*, 2006; Domec *et al.*, 2010; Fu *et al.*, 2012). However, it is not always clear whether embolism resistance measurements in some of these earlier studies were affected by vessel size-related measurement artefacts (cf. Wheeler *et al.*, 2013; Lamarque *et al.*, 2018). While vessel diameters tend to show a general pattern of widening from the leaves towards the roots (Olson *et al.*, 2014; Rosell *et al.*, 2017), studies focusing on patterns in embolism resistance between plant organs within a single plant show less consistent results, indicating that diameter– $P_{50}$  relationships within individual plants do not always follow the interspecific trend. Some authors report leaves (Creek *et al.*, 2018; Skelton *et al.*, 2019) or roots (Maherali *et al.*, 2006; Pratt *et al.*, 2015) to be more vulnerable than stems, some found similar embolism resistance in roots, stems and leaves (Skelton *et al.*, 2017; Wason *et al.*, 2018; Lübke *et al.*, 2022), while others reported leaves to be more resistant than stems (Klepsch *et al.*, 2018; Levionnois *et al.*, 2020; Guan *et al.*, 2022). Finally, microCT observations of intact plants tend to show no (cf. Choat *et al.*, 2016) or inconsistent relationships between vessel diameter and embolism resistance (Losso *et al.*, 2019).

Studies on relationships between wood traits tend to be based on aggregate variables. Before analysis, observations from single vessels or pit membranes are usually averaged across samples, individual trees or species. These levels of aggregation correspond to different observational units that are influenced by mechanisms acting on different scales (Clark *et al.*, 2011), which may partially explain aforementioned differences in outcomes between studies. The choice of the adequate level of aggregation to answer a research question can have profound consequences for the interpretation of a dataset and may result in very different interpretations of the same data (Pollet *et al.*, 2015). The question whether individual trees of the same species with different average vessel diameters differ in embolism resistance, or whether species with different average vessel diameters differ in embolism resistance at the interspecific level, may have fundamentally different answers (cf. Poorter *et al.*, 2018). So far, it is unknown to what extent the interpretation of embolism risk–vessel diameter relationships can be affected by these scale and aggregation issues.

Here, we investigate wood anatomical and hydraulic traits related to embolism resistance in a dataset of 77 tree individuals belonging to 20 temperate broad-leaved tree species. Additionally,

we focus on within-species patterns based on a dataset of 22 *Acer monspessulanum* trees. For both datasets, embolism resistance and wood anatomical traits were derived from the same upper canopy branches, and all trees were sampled at a consistent sampling height. Our design thus intended to minimize confounding effects of tree height- and flow path length-related patterns in vessel size. We use these datasets to address the questions whether embolism resistance (as measured by  $P_{50}$ ) is related to hydraulically weighted vessel diameter ( $D_h$ ), how it relates to pit membrane thickness ( $T_{PM}$ ), and how the answer to these questions is affected by choices during the data analysis. We hereby focus on: whether or not an effect of  $D_h$  on  $P_{50}$  remains after accounting for the confounding effect of  $T_{PM}$ ; to which extent the range of  $D_h$  covered by the species and samples studied may affect the outcome; and whether the observed relationship between  $P_{50}$  and  $D_h$  is consistent within and between species. To achieve the latter, we propose a simple statistical model to decompose trait relationships into intra- and inter-specific components.

## Materials and Methods

### Study site and plant material

For this study, 77 trees from 20 temperate and diffuse-porous angiosperm tree species from 10 genera (Table 1) were chosen from the nursery in the Stutel-Arboretum from the Bavarian State Institute for Viticulture and Horticulture (LWG) at Veitshöchheim, Germany (49°51'49"N, 9°51'8"E). Additionally, 22 *Acer monspessulanum* trees were selected from the Botanical Garden of the University of Würzburg, Germany. The long-term mean annual temperature and mean annual precipitation are 10.0°C and 591 mm in Veitshöchheim and 9.6°C and 560 mm in Würzburg, respectively (Bavarian State Institute for Agriculture – LFL), constituting a continental climate according to the Köppen classification (Peel *et al.*, 2007).

Plant material from the Stutel-Arboretum was collected during June–September 2019 and 2020 (Table 1) from trees aged *c.* 11 yr. Two samples each were taken from 2 to 4 individuals per species. Plant material from the 22 *Acer monspessulanum* trees was collected during November–December 2020 before the onset of frost. Three replicate samples were taken per tree, resulting in a total of 66 samples, two of which had to be discarded due to measurement problems. At both sites, at least 60 cm long twigs were cut from the middle canopy at a height of *c.* 4–5 m, wrapped in wet paper towels, bagged in dark, humidified plastic bags, transported to the laboratory and processed on the same day. For the trees from Stutel, we measured vulnerability curves and wood anatomical traits on one sample, and hydraulic conductivity on the other. The age of the branches at the basal end (determined from microtome slides) was on average 3.7 yr (range: 2–7 yr) for the Stutel site, and on average 7.7 yr (range: 3–15 yr) for the botanical garden.

### Quantification of xylem hydraulic conductivity

For measuring branch xylem hydraulic conductivity ( $K_h$ ; kg m s<sup>−1</sup> MPa<sup>−1</sup>), fresh samples were allowed to rehydrate in water for

**Table 1** Tree characteristics sorted by family.

Family	Species	Code	$n_{\text{tree}}$	DBH (cm)	Height (m)
Betulaceae	<i>Betula pendula</i> Roth	BEPE	4	10.7 ± 1.2	8.4 ± 0.8
	<i>Betula utilis</i> D. Don	BEUT	4	8.6 ± 0.7	6.6 ± 0.3
	<i>Carpinus betulus</i> L.	CABE	4	10.9 ± 0.9	7.4 ± 0.3
	<i>Crataegus persimilis</i> Sarg.	CRPE	4	7.2 ± 0.4	5.9 ± 0.1
	<i>Ostrya carpinifolia</i> Scop.	OSCA	4	8.9 ± 0.2	6.0 ± 0.2
Malvaceae	<i>Tilia cordata</i> Mill.	TICO	4	11.4 ± 0.8	6.5 ± 0.4
	<i>Tilia mongolica</i> Maxim.	TIMO	4	8.8 ± 0.3	5.1 ± 0.1
	<i>Tilia platyphyllos</i> Scop.	TIPL	4	12.2 ± 0.3	7.6 ± 0.2
	<i>Tilia tomentosa</i> Moench	TITO	4	17.2 ± 1.0	7.5 ± 0.5
Platanaceae	<i>Platanus orientalis</i> L.	PLOR	4	11.8 ± 0.9	7.7 ± 0.1
	<i>Platanus × acerifolia</i> (Aiton) Willd.	PLAC	4	9.6 ± 0.6	4.7 ± 0.4
Rosaceae	<i>Prunus padus</i> L.	PRPA	3	10.7 ± 0.8	6.4 ± 0.1
	<i>Prunus serrulata</i> Lindl.	PRSE	4	11.7 ± 0.5	5.8 ± 0.4
	<i>Pyrus calleryana</i> Decne.	PYCA	4	11.2 ± 1.0	7.6 ± 0.8
	<i>Sorbus latifolia</i> (Lam.) Pers.	SOLA	4	9.2 ± 0.7	5.6 ± 0.3
	<i>Sorbus × thuringiaca</i> (Nyman) Schönach.	SOTH	4	9.4 ± 0.6	5.9 ± 0.3
Sapindaceae	<i>Acer campestre</i> L.	ACCA	4	10.8 ± 0.6	7.0 ± 0.2
	<i>Acer monspessulanum</i> L.	ACMO	2 (22)	12.6 ± 0.7	6.7 ± 0.1
	<i>Acer platanoides</i> L.	ACPL	4	12.3 ± 0.7	7.2 ± 0.2
	<i>Acer rubrum</i> L.	ACRU	4	8.7 ± 0.6	6.2 ± 0.2

Given are the family, species name, sample code used in subsequent figures, number of sampled individuals ( $n_{\text{tree}}$ , with the number of trees from the Würzburg botanical garden in brackets for *A. monspessulanum*) and the mean and SD of diameter at breast height (DBH) and tree height (Height).

at least 20 min and then recut under water from both ends to a length of 35 cm, which exceeds the maximum vessel length for all species analysed (S.S. Paligi & R.M. Link, unpublished). Subsequently, lateral twigs were removed and the cuts immediately sealed using quick-drying adhesive (Loctite 431 with activator 7452; Henkel, Düsseldorf, Germany) to prevent leakage. Then, the samples were connected to a Xyl'em Plus embolism meter (Bronkhorst, Montigny-Les-Cormeilles, France) with silicone tubes to measure stem hydraulic conductivity using degassed, demineralized water containing 10 mM KCl and 1 mM  $\text{CaCl}_2$ . After measuring initial hydraulic conductivity at a low-pressure head of 6 kPa for 5 min, samples were repeatedly flushed at high pressure of 120 kPa for 10 min to remove emboli to measure maximum hydraulic conductivity once the conductivity values were stable. Hydraulic conductivity was calculated as  $K_h = f \times L / \Delta P$ , where  $f$  ( $\text{kg s}^{-1}$ ) is the flow rate, and  $\Delta P$  (MPa) is the pressure drop along the length of the segment ( $L$ , m). The specific conductivity ( $K_s$ ;  $\text{Kg m}^{-1} \text{MPa}^{-1} \text{s}^{-1}$ ) was then computed by dividing the observed maximum  $K_h$  by the basal cross-sectional xylem area ( $A_{\text{cross}}$ ,  $\text{m}^2$ ), excluding bark.

### Vulnerability curves with the flow-centrifuge method

Vulnerability curves based on the flow-centrifuge method were measured with a Cavitrone device (Cochard *et al.*, 2005) built from a Sorval RC 5 centrifuge with manual control of rotation speed, and using the CAVISOF software (CAVISOF v.5.2.1, University of Bordeaux, Bordeaux, France). A subset of the vulnerability curves in this paper was also used for a methodological comparison with the pneumatic method (Paligi *et al.*, 2021).

In total, vulnerability curves were constructed for 77 branches from the Stutel-Arboretum (basal diameter: mean ± SD

8.87 ± 0.88 mm; Supporting Information Fig. S1) and 64 *Acer monspessulanum* branches from the botanical garden (diameter: 7.03 ± 0.82 mm). After sampling, the branches were submerged in demineralized water immediately upon arrival in the laboratory and recut several times using pruning shears to release the negative pressure in the xylem (Torres-Ruiz *et al.*, 2015). Then, lateral twigs were removed and samples shortened to a final length of 27.5 cm. Subsequently, samples of 3–4 cm length were cut from the basal and apical sample end and stored in 70% ethanol for anatomical observations. Before inserting the branch segments in a custom-made rotor, the bark was removed at both stem ends, and their diameters were measured. Conductance was measured using the solution mentioned above, starting at a water potential of −0.834 MPa (equivalent to 3000 rotations per minute) and reducing the water potential stepwise until at least 90% loss of initial conductance recorded with the CAVISOF software. After each increase in rotational velocity and hence in pressure, we waited for 2 min before conductance was measured.

### Vessel anatomical traits from light microscopy

For all species, thin (20 µm) traverse sections of the wood anatomical samples were made with a sliding microtome (G.S.L.1; Schenkung Dapples, Zürich, Switzerland), stained with safranin-alcian blue, rinsed with distilled water and ethanol (95%) and permanently embedded on glass slides using Euparal (Carl Roth, Karlsruhe, Germany). Subsequently, the complete cross-section was digitalized at 100-times magnification using a light microscope equipped with an automated table and a digital camera (Observer.Z1 and Software: AXIOVision v.4.8.2; Carl Zeiss MicroImaging GmbH, Jena, Germany). Anatomical measurements were made by semi-automated image analysis using

IMAGEJ v.1.52p (Schneider *et al.*, 2012) and GIMP v.2.10.6 (GIMP Development Team, 2018). While the majority of vessels could be identified by applying this semi-automated approach, it was impossible to completely exclude tracheids in our measurements of some species because narrow vessels cannot be easily distinguished from tracheids based on transverse sections. The equivalent vessel diameter according to White (1991;  $d$ ,  $\mu\text{m}$ ), that is the diameter of a circular vessel with the same conductivity as an elliptical one with minor and major radius  $a$  and  $b$ , was calculated as:

$$d = \left( \frac{32 (ab)^3}{a^2 + b^2} \right)^{0.25} \quad \text{Eqn 1}$$

Based on  $d$ , the hydraulically weighted average vessel diameter ( $D_h$ ,  $\mu\text{m}$ ) was calculated according to Sperry *et al.* (1994) as:

$$D_h = \frac{\sum d^5}{\sum d^4} \quad \text{Eqn 2}$$

### Pit anatomical traits from transmission electron microscopy

One sample per species was prepared for transmission electron microscope (TEM) analyses to measure pit membrane thickness ( $T_{\text{PM}}$ , nm) following the protocol by Jansen *et al.* (2009).

Small xylem slivers were cut with a fresh razor blade from the two outmost growth rings of the fresh and hydrated wood samples used for hydraulic measurements on the day of sample collection. The slivers were then cut to 1 mm<sup>3</sup> cubes in water and fixed in a standard fixative (5% glutaraldehyde in 0.1 mol cacodylate buffer). Then, the samples were washed in a 50 mmol cacodylate buffer and postfixed in 2% buffered osmium tetroxide in 0.1 mol cacodylate buffer for 2 h in ice. They were then stained with 0.5% uranyl acetate and dehydrated through a gradual ethanol series (30%, 50%, 70% and 90%) for 2–3 min. Samples were embedded in Epon resin (Sigma-Aldrich) at 60°C. Transverse, semi-thin (500 nm thick) sections were cut from the embedded samples with a glass knife, stained with 0.5% toluidine blue in 0.1 mol phosphate buffer and mounted on slides with Eukitt (Plano GmbH, Berlin, Germany). Ultra-thin sections between 60 and 100 nm thick were cut with a diamond knife using an ultra-microtome (Leica Ultracut UCT; Leica Microsystems, Vienna, Austria) and deposited on a copper grid (Athena; Plano GmbH, Wetzlar, Germany). Several grids were prepared for each TEM sample. Intervessel pit membranes were observed under a Jeol 1210 TEM (Jeol Germany GmbH, Freising, Germany) at 120 kV accelerating voltage. TEM pictures were taken with a digital camera (Soft Imaging System, Münster, Germany). IMAGEJ v.1.52p was used to measure  $T_{\text{PM}}$  at least three times per pit membrane at opposite sides near the pit membrane annulus (i.e. close to the pit border) and in the centre. Shrunken pit membranes were excluded because these were likely showing artefacts by deformation, aspiration, or ageing and thus may not represent functional pit membranes (Schmid & Machado, 1968; Sorek *et al.*, 2021). Shrunken pit membranes

were identified based on their electron-dense appearance under TEM, while fresh pit membranes in functional conduits generally have a low electron density, with a homogeneous, granular appearance of lipids on and/or in pit membranes (Zhang *et al.*, 2017, 2020; Kotowska *et al.*, 2020). While intervessel pit membranes were imaged as much as possible, it was not possible to distinguish narrow vessels from tracheids in some species based on a transverse TEM section. Therefore, both intervessel and vessel-tracheid pit membranes may be included in our analyses.

### Statistical analyses

All statistical analyses were performed in R v.4.2.2 (R Core Team, 2022) in the framework of the TIDYVERSE v.1.3.2 (Wickham *et al.*, 2019).

Vulnerability curves were fitted with nonlinear least squares using the logistic model by Pammenter & Vander Willigen (1998) in the modified version based on hydraulic conductivity (Ogle *et al.*, 2009):

$$K_i \approx \text{Normal} \left( K_{\text{sat}} \cdot \left( 1 - \frac{1}{1 + \exp \left( -\frac{S_{50}}{25} (P_i - P_{50}) \right)} \right), \sigma \right), \quad \text{Eqn 3}$$

where for each observation  $i$ , the conductivity  $K_i$  is assumed to be normally distributed with residual SD  $\sigma$  around a logistic function of the water potential  $P_i$  with the parameters  $P_{50}$  (water potential at 50% loss of conductivity),  $S_{50}$  (corresponding slope on the per cent loss of conductivity scale) and  $K_{\text{sat}}$  (conductivity at full saturation).

The significance of linear associations at the species level was tested with linear models of species averages fitted with ordinary least squares. To illustrate the effect of range restriction on regression results, we further fitted an analogous model of  $P_{50}$  vs  $D_h$  with a subsample of species (arbitrarily restricted to a range of  $D_h$  of 35–45  $\mu\text{m}$  for demonstrational purposes). After constructing a directed acyclic graph (DAG; cf. Shrier & Platt, 2008) to identify necessary covariate adjustments, we used multiple linear regression to test whether relationships between  $D_h$  and  $P_{50}$  resulted from a confounding effect of  $T_{\text{PM}}$ , or whether a diameter effect remained after accounting for  $T_{\text{PM}}$ .

To illustrate the importance of the level of aggregation for the interpretation of relationships between plant traits, we further fitted two models of  $P_{50}$  at the individual level. We hereby contrasted the classical linear mixed-effects model (LME) formulation with random intercepts and slopes with a modified LME that used *within-species centring* to separate within- and between-species effects of  $D_h$  analogous to the within-subject centring in van de Pol & Wright (2009). In the classical formulation, the dependent variable  $y_i$  for each observation  $i$  in  $(1 \dots N)$  is expressed as a linear function of the predictor variable  $x_i$  with intercept  $\alpha$  and slope  $\beta$ , which are allowed to vary for each group  $j$  in  $(1 \dots J)$ :



$$y_i = (\alpha + u_j) + (\beta + v_j) \cdot x_i + \epsilon_i \quad \text{Eqn 4}$$

Here,  $\epsilon_i$  are the model residuals, while  $u_j$  and  $v_j$  are the species-wise random deviations from the overall average parameters, and usually modelled as realizations of a multivariate normal distribution with a covariance matrix estimated from the data. The slope  $\beta$  estimated by this model is only a valid estimate of the average intraspecific slope if there is no between-species variation in  $x$  (cf. Bafumi & Gelman, 2007; van de Pol & Wright, 2009), a condition that is likely not met by most studies of relationships between evolutionarily constrained traits. Moreover, this model provides no estimate of the interspecific slope, which often may be equally or more relevant than the intraspecific slope.

We contrasted the model in (4) with an LME with within-species centring, an alternative formulation that separates the effect of the predictor variable  $x_i$  into the species averages  $\bar{x}_j$  and the deviations from these averages ( $x_i - \bar{x}_j$ ). This allowed us to decompose the relationship studied into an across-species and a within-species component with separate parameters  $\beta_{\text{across}}$  and  $\beta_{\text{within}}$ .

$$y_i = (\alpha + u_j) + \beta_{\text{across}} \cdot \bar{x}_j + (\beta_{\text{within}} + v_j) \cdot (x_i - \bar{x}_j) + \epsilon_i \quad \text{Eqn 5}$$

The models in Eqns 4, 5 were fitted in a Bayesian hierarchical modelling framework with moderately informative priors (cf.

Lemoine, 2019) using the R package BRMS v.2.18.0 (Bürkner, 2017, 2018; see Notes S1 for details).

## Results

### Embolism resistance, hydraulic efficiency and wood anatomy across species

Our results covered a wide interspecific range of xylem embolism resistance measured as the xylem water potential at 50% loss of hydraulic conductivity ( $P_{50}$ ), specific hydraulic conductivity ( $K_s$ ) and hydraulically weighted vessel diameter ( $D_h$ ) in the branch xylem. In our study, across 20 temperate, diffuse-porous and broad-leaved tree species ( $n = 77$ ),  $P_{50}$  varied from  $-7.33$  to  $-1.70$  MPa,  $K_s$  from  $0.46$  to  $1.98 \text{ kg m}^{-1} \text{ MPa}^{-1} \text{ s}^{-1}$  and  $D_h$  from  $25.25$  to  $45.17 \text{ }\mu\text{m}$  (Figs 1, S2; Table S1). Within *Acer monspessulanum* ( $n = 66$ ),  $P_{50}$  ranged from  $-7.99$  to  $-6.00$  MPa and  $D_h$  from  $25.9$  to  $35.4 \text{ }\mu\text{m}$ .

In analyses of interspecific bivariate relationships (Fig. 2a,b; Table S2), species with a higher  $D_h$  had a less negative  $P_{50}$  and hence a lower embolism resistance ( $R^2 = 0.50$ ,  $P < 0.001$ ), while species with a higher pit membrane thickness ( $T_{\text{PM}}$ ) were more embolism-resistant ( $R^2 = 0.51$ ,  $P = 0.001$ ).  $P_{50}$  further increased significantly with  $K_s$  ( $R^2 = 0.47$ ,  $P = 0.001$ ), that is species with high xylem conductivity tended to have low embolism resistance (Fig. 2c; Table S2).

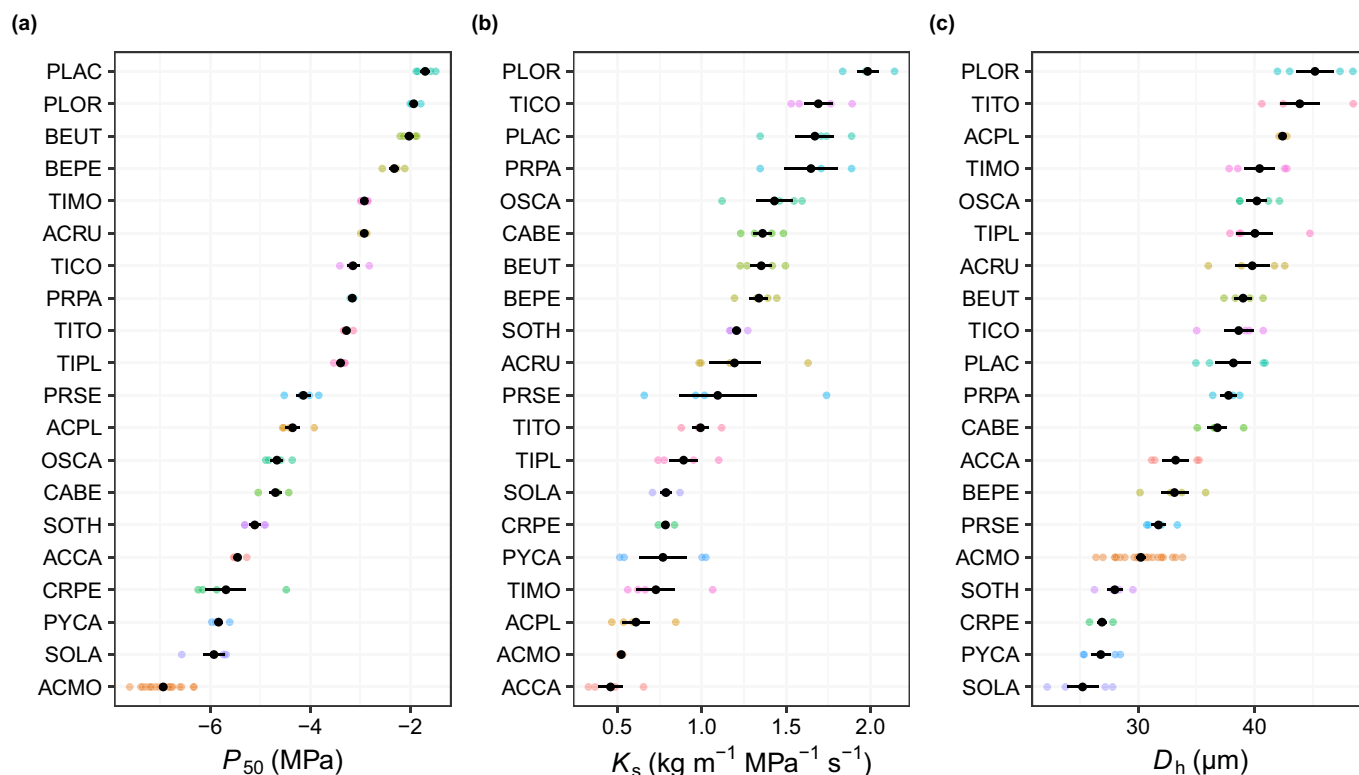


**Fig. 1** Observed ranges of (a) the water potential at 50% loss of conductivity ( $P_{50}$ ), (b) the maximum specific conductivity ( $K_s$ ) and (c) the hydraulically weighted vessel diameter ( $D_h$ ) of 20 angiosperm tree species, with 3–4 (*Acer monspessulanum*: 24) individuals per species. Shown are raw data from individual plants (points, colored by species) overlaid with mean  $\pm$  SE (black points and lines), ordered by their mean values. For species codes, see Table 1.

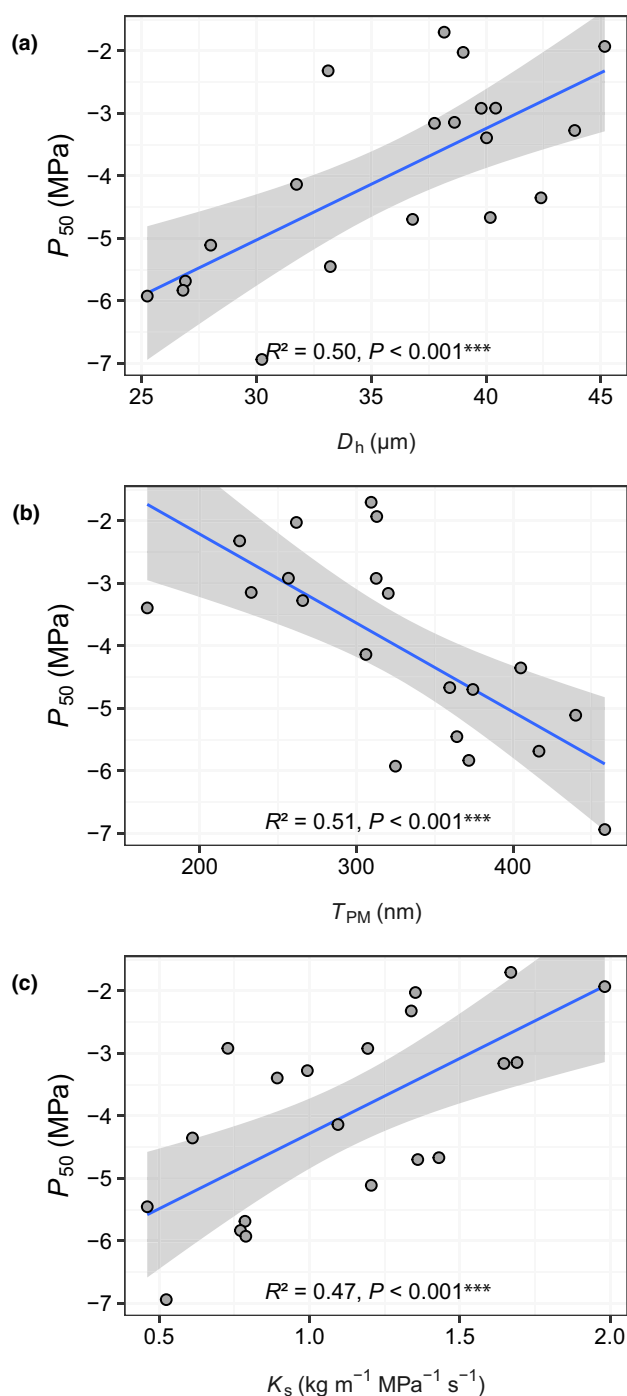


**Fig. 2** Results of simple species-level linear regressions of water potential at 50% loss of conductivity ( $P_{50}$ ) vs (a) hydraulically weighted vessel diameter ( $D_h$ ), (b) pit membrane thickness ( $T_{PM}$ ) and (c) maximum specific conductivity ( $K_s$ ). Shown are the species-level averages (grey points) overlaid with the model predictions (blue line)  $\pm$  95% confidence bands (grey area). For regression parameters, see Supporting Information Table S2.

### Determinants of embolism resistance

The hypothesized relationships between  $D_h$ ,  $T_{PM}$  and  $P_{50}$  are reflected in the DAG in Fig. 3(a), with the potential indirect

path via the unobserved intervessel pit area displayed in grey. While there was a significant negative correlation between  $D_h$  and  $T_{PM}$  ( $r = -0.463$ ,  $t = -2.215$ ,  $df = 18$ ,  $P = 0.039$ ), the direction and magnitude of this link were not nearly sufficient to explain the association observed between  $D_h$  and  $P_{50}$ . A key result is that a sizeable positive effect ( $P = 0.006$ ) of  $D_h$  on  $P_{50}$  remained after accounting for the negative effect of  $T_{PM}$  ( $P = 0.005$ ), that is species with the same value of  $T_{PM}$  were more embolism-resistant when they had narrower vessels (Fig. 3b,c; Table S2). Together,  $D_h$  and  $T_{PM}$  explained 68.9% of the variance in species-level  $P_{50}$ . At the sample level,  $P_{50}$  was not significantly correlated with sample age, neither for the Stuel dataset ( $r = -0.032$ ,  $t = -0.277$ ,  $df = 75$ ,  $P = 0.782$ ), nor for the *Acer monspessulanum* dataset ( $r = -0.126$ ,  $t = -1.001$ ,  $df = 62$ ,  $P = 0.321$ ).

### Importance of trait value range and the level of aggregation

The range of trait values covered was found to strongly affect the results obtained (Fig. 4a), with the slope of a linear regression explaining 50% of the variance in the full species-level dataset ( $P < 0.001$ ), and only 2% in a subset arbitrarily limited to a range of  $D_h$  between 35 and 45  $\mu\text{m}$  ( $P = 0.676$ ; Fig. 4a; Table S2). Moreover, there was no evidence for a significant intraspecific association of  $P_{50}$  with  $D_h$  ( $R^2 < 0.001$ ,  $P = 0.961$ ; Fig. 4b; Table S2) for the 22 individual *Acer monspessulanum* trees.

The outcomes of analyses of trait relationships on the individual level were strongly affected by model specification. Fig. 5 contrasts two alternative specifications for LME models of the association between  $P_{50}$  with  $D_h$  based on individual-level data. It is clear that the regular random intercept and slope formulation (Eqn 4) was not able to recover the interspecific association observed (Fig. 5a). The slope for the overall trend in this model was not credibly different from zero (slope 0.019, 95% credible interval:  $-0.015$  to  $0.053$ ; Table S3). In the model formulation with within-species centring (Eqn 5), we found evidence for a strong positive effect of  $D_h$  on species level (slope 0.177, 95% CI:  $0.085$ – $0.267$ ), while the average within-species slope was not credibly different from zero (0.007, 95% CI:  $-0.029$  to  $0.042$ ; Table S3; Fig. 5b).

### Discussion

Our results provide evidence for an interspecific relationship of xylem embolism resistance (as measured by the  $P_{50}$ -value) with both pit membrane thickness ( $T_{PM}$ ) and hydraulically weighted vessel diameter ( $D_h$ ) in the branch xylem of temperate diffuse-porous angiosperm trees. They further demonstrate that a potential link between vessel diameter and pit membrane thickness cannot explain the lower embolism resistance of species with wider vessels. As such, our data provide clear evidence that in the species studied, vessel dimensions have an effect on embolism resistance, and that this relationship cannot be explained by pit membrane thickness only.

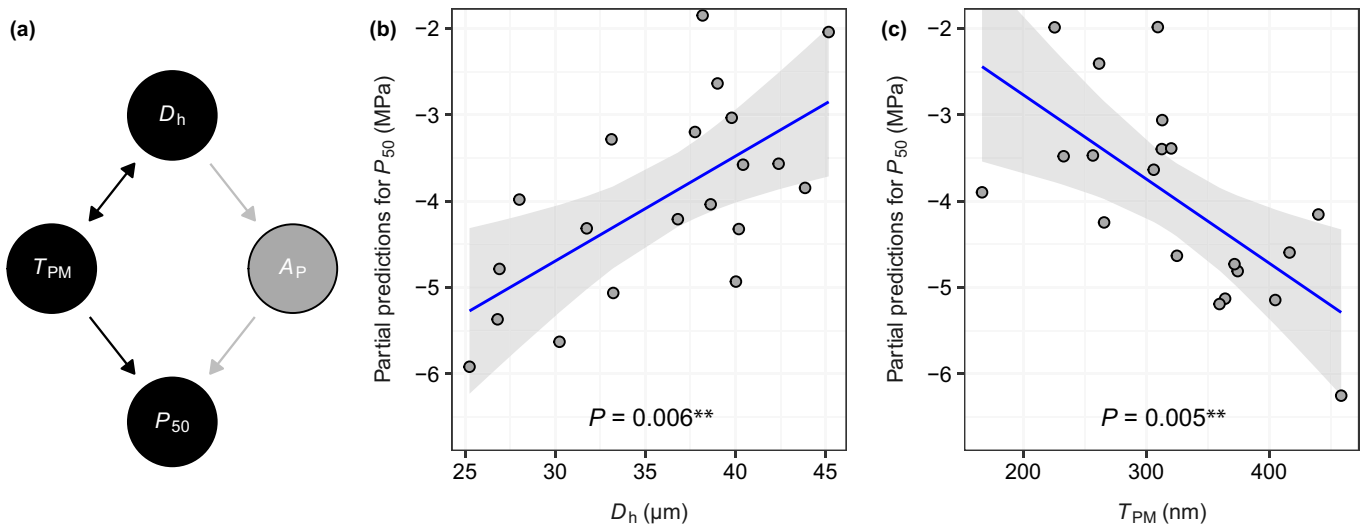


**Fig. 3** Alternative way of looking at the relationships between  $D_h$ ,  $T_{PM}$  and embolism resistance. Left (a): directed acyclic graph for the relationships between water potential at 50% loss of conductivity ( $P_{50}$ ), pit membrane thickness ( $T_{PM}$ ), hydraulically weighted vessel diameter ( $D_h$ ) and total pit surface area ( $A_P$ ). Unidirectional arrows: causal relationships, bidirectional arrows: correlative associations. The grey arrows indicate the potential indirect effect of  $D_h$  on embolism safety via the unmeasured intervessel pit area per vessel (grey). Right: Partial predictions from a multiple regression model of  $P_{50}$  vs (b)  $D_h$  and (c)  $T_{PM}$ . Shown are counterfactual predictions for  $P_{50}$  (predictions for one variable when the other variable is held at its average value; blue lines) with 95% confidence bands (grey area), overlaid with partial residuals (grey points). For regression parameters, see Supporting Information Table S2.

### The role of pit membrane thickness in embolism resistance

The important role of pit membrane properties for embolism resistance has been demonstrated in various studies (Choat *et al.*, 2003; Lens *et al.*, 2011, 2013; Scholz *et al.*, 2013; Li *et al.*, 2016; Kaack *et al.*, 2021). In our dataset, tree species with thicker intervessel pit membranes were more resistant to drought-induced embolism than species with thinner pit membranes (Fig. 2), which is in accordance with previous reports for angiosperm species both at the interspecific and intraspecific level (Lens *et al.*, 2011; Scholz *et al.*, 2013; Li *et al.*, 2016; Schuldt *et al.*, 2016).

A mechanistic explanation for the relationship between embolism resistance and  $T_{PM}$  is that due to the link between the thickness and pore size distribution of nonwoven fibrous media (cf. Bai *et al.*, 2020), thicker pit membranes can be expected to have narrower maximum sizes of pore constrictions. If embolism formation is triggered by air passing through pore constrictions, thicker pit membranes should therefore result in reduced embolism risk (Jansen *et al.*, 2018). The rare pit hypothesis assumes that a vessel's embolism risk depends on the size of its largest pore, which is predicted to be linked to its total pit area ( $A_P$ ) and hence vessel dimensions (Hargrave *et al.*, 1994; Wheeler *et al.*, 2005). A corollary of this hypothesis is therefore that for given values of  $A_P$ , species with thicker pit membranes should have a higher embolism resistance (cf. Christman *et al.*, 2009).

However, it has been pointed out that the rare pit hypothesis is based on a two-dimensional view of pit membranes that does not capture the complexity of their spatial structure (Kaack *et al.*, 2019). Models of air-seeding processes based on the Young–Laplace equation implicitly assume pit membranes to consist of a set of circular, parallel pores with constant diameter that connect both sides of the membrane. In reality, the pore

space between cellulose microfibrils of pit membranes forms a large, highly interconnected pathway consisting of multiple pore spaces and narrow pore constrictions (Zhang *et al.*, 2020). In agreement, mechanistic modelling and experimental data show that the minimum pore constrictions in pit membranes are smaller than expected, and leaky pit membranes are by far not common enough to support the rare pit hypothesis (Kaack *et al.*, 2021). In addition, the presence of stable gas nanobubbles in the xylem sap (Schenk *et al.*, 2015, 2017), dynamic changes in surface tension induced by local concentration gradients of insoluble lipid-based surfactants (Yang *et al.*, 2020) and uncertainties regarding the mechanisms that drive the spontaneous snap-off of gas bubbles at the air–water interface in membrane pore constrictions (Park *et al.*, 2019) put into question whether direct bubble penetration as based on the air-seeding hypothesis really is the main mechanism behind embolism formation (Kaack *et al.*, 2021). Indeed, pressure-driven gas diffusion across pit membranes may be as important for the spread of emboli as the bulk flow of gas implied by air-seeding (Guan *et al.*, 2021). If the driving process for the formation of emboli is the spontaneous expansion of previously stable gas bubbles that either entered vessels as nanobubbles, or came out of solution, pit membrane thickness can be expected to have a strong effect on embolism resistance via its link to permeability. However, in this case, it is less clear why  $P_{50}$  should be associated with vessel dimensions (Lens *et al.*, 2022).

### How can we explain the $P_{50}$ – $D_h$ relationship mechanistically?

One potential reason for the observed link between  $P_{50}$  and  $D_h$  is the dependence of embolism resistance on the connectivity of the

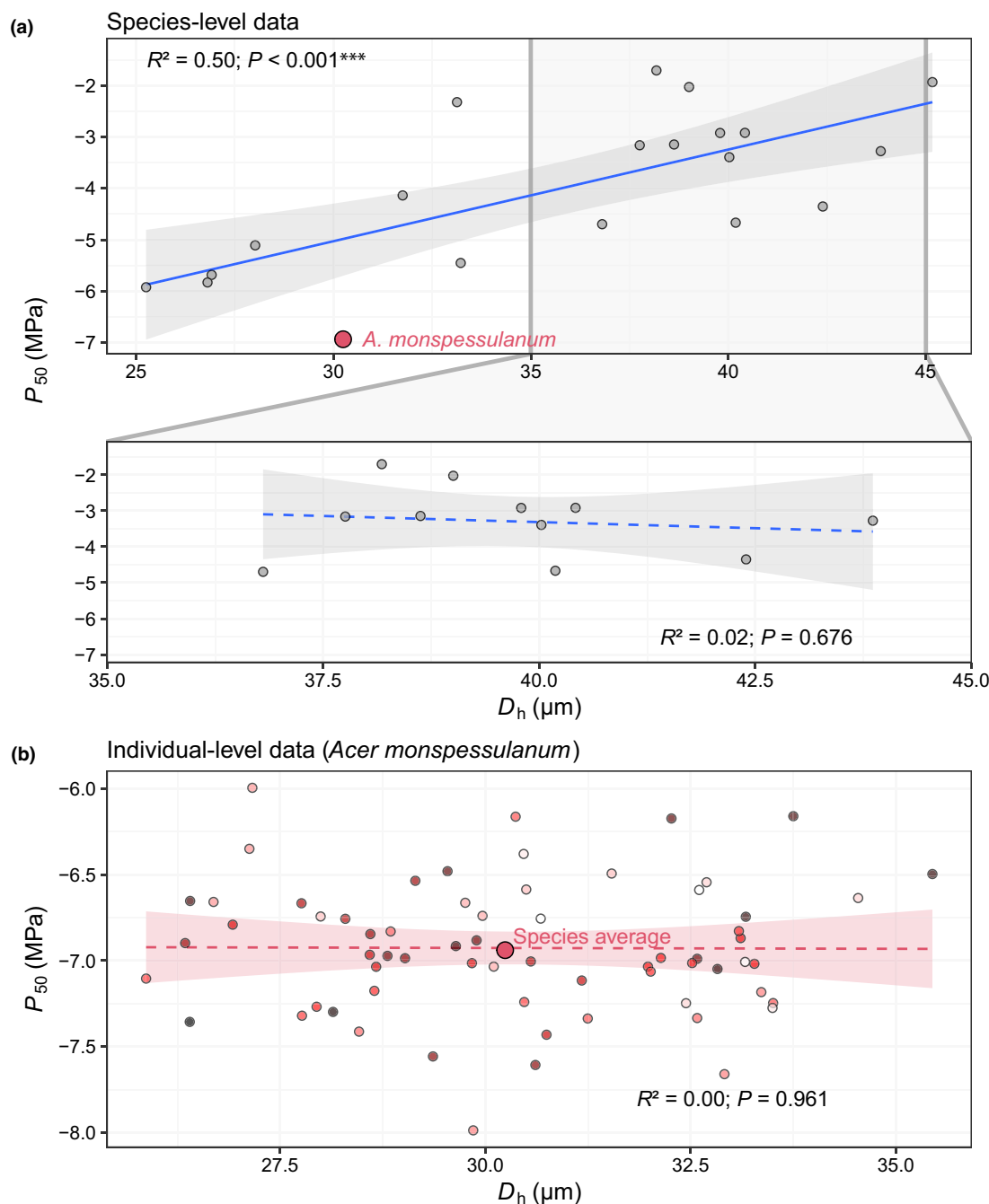


**Fig. 4** Range of observations and the observational scale can affect the observed  $P_{50}$ – $D_h$  relationships. (a) Effect of range restriction on the outcome of a linear regression. The upper panel shows the full range of the data shown in the first panel of Fig. 2 with the explained variance and  $P$ -value in a linear regression, while the lower panel is based only on observations with a  $D_h$  between 35 and 45  $\mu\text{m}$ . Shown are the species-level observations (points) overlaid with the linear regression predictions (blue) and 95% confidence bands (grey area). (b) Within-species relationship of *Acer monspessulanum* of water potential at 50% loss of conductivity ( $P_{50}$ ) vs hydraulically weighted vessel diameter ( $D_h$ ). Shown are sample level measurements (points, colored by tree individual) overlaid with a linear regression line and its 95% confidence bands. For regression parameters, see Supporting Information Table S2.

conduit network, including vessels and tracheids (Loepfe *et al.*, 2007; Mrad *et al.*, 2018, 2019; Wason *et al.*, 2021). If larger vessels have a higher connectivity, that is if each vessel shares bordered pits with a higher number of other vessels or tracheids as potential sources of embolism spread, this may constitute a link between embolism resistance and vessel dimensions,

independent of the frequency of rare, leaky pits (cf. Levionnois *et al.*, 2021).

The probabilistic argument that is at the core of the rare pit hypothesis (Christman *et al.*, 2009) can also be extended to processes other than bulk flow of bubbles through pit membranes. Embolism formation is a highly nonlinear process, where a slight



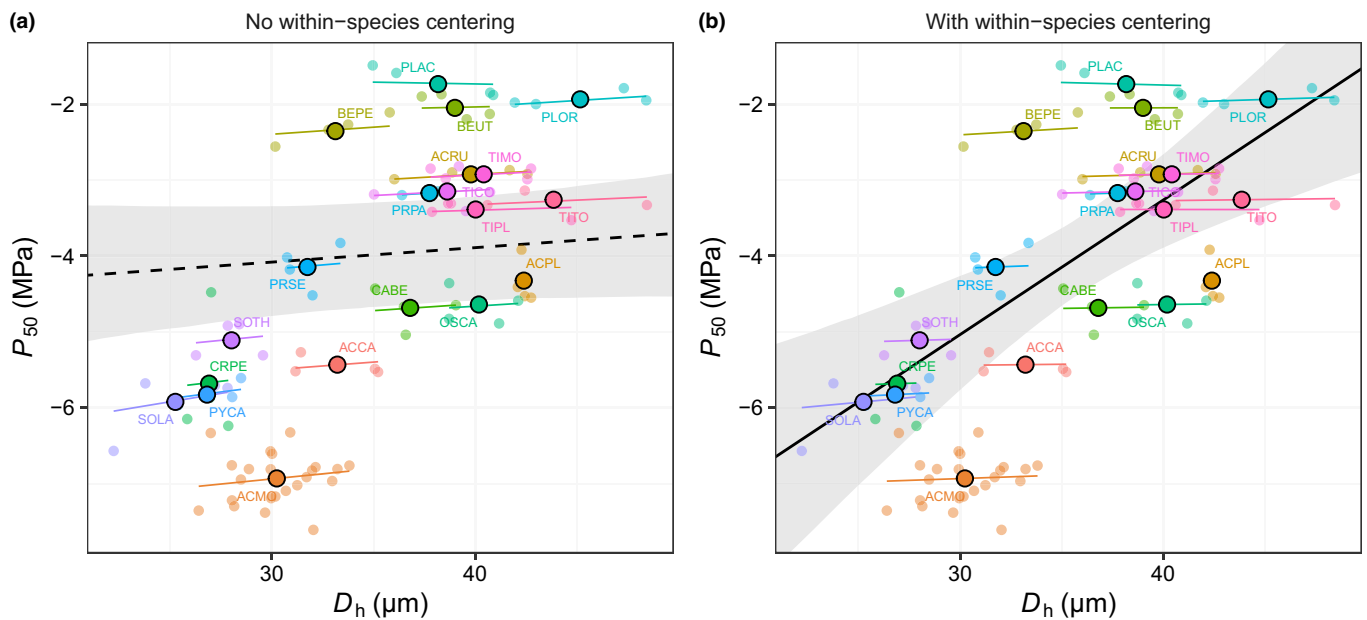


**Fig. 5** Dependence of trait relationships on the aggregational level and the implications of within-species centring for overall and species-specific predictions. (a) Predictions from a mixed-effects model using a regular random slope and intercept formulation (Eqn 4). (b) Within- and between-species predictions from a mixed model with random intercepts and slopes using within-species centring (Eqn 5). Shown are the raw data (small points) and species averages (big points with black contour) overlaid with marginal predictions (black) with 95% credible intervals (grey) as well as conditional within-species predictions (coloured lines). For species codes, see Table 1; parameter estimates are provided in Supporting Information Table S3.

state change can trigger the complete and largely irreversible loss of conductive function of a vessel once a certain tipping point has been crossed (cf. Arend *et al.*, 2021; Johnson *et al.*, 2022). If embolism formation depends on a stochastic process that can happen with a certain probability anywhere in a vessel, it is more likely to happen *at least once* in a vessel with a larger volume, which therefore will invariably possess a higher embolism risk. Importantly, this applies to all the drivers of embolism formation depending on gas dynamics discussed above. If embolism formation, for instance, was driven predominantly by the expansion of nanobubbles that exceed a critical size (Schenk *et al.*, 2017; Park *et al.*, 2019; Ingram *et al.*, 2021), a single bubble exceeding this threshold size would be sufficient to cause the complete loss of functionality of the corresponding vessel. Similarly, if emboli spread predominantly via gas diffusion through pit membranes (Guan *et al.*, 2021), it would only take one large enough bubble coming out of solution, for example after a temperature increase (see fig. 1 in Schenk *et al.*, 2016), to trigger a catastrophic state change. As both processes are more likely to happen at least once in larger xylem sap volumes, they are consistent with a link between embolism resistance and vessel dimensions that is independent of  $A_p$ . Notably, none of these processes are mutually exclusive, and the formation and spread of emboli is likely driven to some extent by diffusion from adjacent, embolized vessels, nanobubbles entering through pits and, in some cases, potentially also bubble penetration through faults in pit membranes resulting for example from mechanical damage. As all processes mentioned above depend on the occurrence of rare events that are hard to observe, the possibility for empirical testing of their influence is limited (Kaack *et al.*, 2019). The most promising way of

evaluating their importance is therefore via mechanistic modelling approaches as in Kaack *et al.* (2021). If the processes of interest for embolism formation depend on the occurrence of rare events situated in the extreme tails of highly skewed probability distributions, a promising route to improve existing models may be to guide them by basic principles of extreme value theory (Coles *et al.*, 2001; Reiss & Thomas, 2007). A recent application in an ecophysiological context is provided by Martínez-Vilalta *et al.* (2021), who proposed the use of methods from this field to improve estimates of minimum water potentials.

If embolism resistance indeed depended on vessel diameter, this relationship would establish a mechanistic link between plant drought responses and pervasive trends in wood anatomy. This provides a potential explanation for both large-scale patterns in the variation in vessel diameter along climate gradients (Pfautsch *et al.*, 2016; Hacke *et al.*, 2017) and patterns observed in growth rings of years differing in water availability (Zimmermann *et al.*, 2021). Moreover, given the universal scaling of vessel diameter with path length within individuals (Olson *et al.*, 2014), the existence of a xylem safety–vessel diameter relationship may help explain the higher embolism risk of taller plants (Anfodillo & Olson, 2021), and thus why water availability dictates global patterns in plant height (Moles *et al.*, 2009). In addition, the link between  $D_h$  and  $P_{50}$  is at the basis of a potential hydraulic safety–efficiency trade-off (Hacke *et al.*, 2006). Indeed, our results showed a positive relationship between  $P_{50}$  and specific conductivity ( $K_s$ ), with more embolism-resistant species having less efficient xylem (Fig. 2c). Notably, the correlation between  $P_{50}$  and  $K_s$  observed here is strong compared with other values reported in the literature (Gleason *et al.*, 2016; van der Sande *et al.*, 2019;

Lübbe *et al.*, 2022). This strong link may result from using a sample of similarly sized trees from species with diffuse-porous wood covering a broad range of embolism resistance (Fig. 1), grown under identical conditions and measured with consistent methods, which highlights the importance of controlled experimental conditions to minimize the influence of confounding covariates.

### Reconciling discrepancies about the vessel diameter–embolism resistance relationship

One potential explanation for inconsistency in the literature about the  $D_h$ – $P_{50}$  relationship is bias induced by missing covariates (Shrier & Platt, 2008), most importantly pit membrane thickness. In our dataset, we observed a strong  $D_h$ – $P_{50}$  relationship (Figs 3–5). While a spurious association induced by a link between  $D_h$  and  $T_{PM}$  could be ruled out for our dataset, it is possible that an unaccounted positive  $D_h$ – $T_{PM}$  relationship may mask an existing relationship in other datasets, especially when covering wider ranges of species with different pit morphologies. In either case, it is important to point out that tests of bivariate associations (cf. Fig. 2) and regression models with more than one predictor (cf. Fig. 3) answer fundamentally different questions. While the former is a sensible approach when the question is whether and how two traits are associated, the study of pairwise bivariate associations is generally not an adequate tool for inference about causal relationships between variables, for example whether or not one trait has an effect on another trait (cf. Pearl, 2000). If the latter is desired, it may be more adequate to use graphical approaches based on DAGs (cf. Fig. 3a; Greenland *et al.*, 1999; Shrier & Platt, 2008) to identify the variables that have to be included in multiple regression models, or to employ formal causal inference frameworks such as structural equation modelling (Grace *et al.*, 2012). One central takeaway from the DAG in Fig. 3(a) is that if  $T_{PM}$  and  $D_h$  are correlated, it is impossible to obtain unbiased evidence about the existence of a  $D_h$ – $P_{50}$  link without accounting for  $T_{PM}$ .

A second potential explanation why some studies report a link between  $D_h$  and  $P_{50}$ , while others do not, are differences in the range of trait values covered. As illustrated in Fig. 4(a), even if the  $D_h$ – $P_{50}$  relationship remains identical, a restricted range in the traits sampled results in a lower power to detect an existing relationship (Bland & Altman, 2011). Hence, a weak correlation between two traits is insufficient to conclude that there is no relationship if the sampling covers only a small part of the potential variation of these traits. For instance, to identify a true relationship based on a Pearson correlation test with a nominal power of 0.8 and a significance level of 0.05 for an identical slope as in Fig. 4(a), one would need 12.4 observations, but 40.6 observations (i.e. over three times more) would be required for an equally strong relationship if  $D_h$  was constrained to values between 35 and 45  $\mu\text{m}$  (calculated with R package *PWR* v.1.3-0; Champely, 2020). Accordingly, studies covering a restricted range of one or more traits are less likely to be able to identify an existing relationship. This is especially relevant for studies of intraspecific patterns, as hydraulic safety-related traits are

evolutionarily conserved traits (Hajek *et al.*, 2016; Fuchs *et al.*, 2021; Weithmann *et al.*, 2021) and hence have a limited range within species.

A third – and perhaps the most relevant – factor contributing to disparate results in studies of xylem safety–vessel diameter relationships is the dependence of trait relationships on the level of data aggregation. Our dataset illustrates that trait relationships are not consistent across levels of aggregation, and that a strong interspecific pattern can be consistent with the complete absence of any intraspecific relationships between the same traits (Fig. 5b). While trait relationships are often analysed at the species level, most processes that determine the fitness of plants, like competition and plant–environment interactions, act at the individual level (Clark *et al.*, 2011). However, when focusing on the individual level, the trait relationships observed may be obscured or even reversed by ontogenetic trends, size-related constraints or variation across organs (cf. Li *et al.*, 2019; Zimmermann *et al.*, 2021; Lübbe *et al.*, 2022). For example, a major driver of intraspecific variability in  $D_h$  is the widening of vessels along the flow path, which tends to follow relatively static scaling relationships (Olson *et al.*, 2014; Rosell *et al.*, 2017). If not properly controlled or accounted for, these intra-individual patterns in  $D_h$  may mask existing relationships with  $P_{50}$  at the individual or species level. This would especially be the case if  $T_{PM}$  changed along the flow path (Kotowska *et al.*, 2020; Guan *et al.*, 2021). Accounting for size effects that drive intratree and intraspecific variation is especially relevant when analysing trait associations measured on different observational units, for example the relationship between branch  $P_{50}$  and stem  $D_h$ , or  $D_h$  and  $P_{50}$  measured on different trees with different sizes. The design of this study, which focused on traits measured on the same branch samples and at similar positions along the flow path, permitted us to minimize the effect of these confounding size effects.

The complete absence of a credible intraspecific effect of  $D_h$  on  $P_{50}$  in the presence of a strong interspecific pattern (Fig. 5b) illustrates that for analyses of trait relationships it is crucial to consider on which level of aggregation inference is desired. Importantly, conflating inference on different levels of aggregation is not merely imprecise, but constitutes a logical fallacy (ecological/individualistic fallacy) that may lead to erroneous conclusions (cf., Robinson, 1950; Subramanian *et al.*, 2009; Pollet *et al.*, 2015).

As illustrated in Fig. 5, the classical random slopes and intercepts LME only estimates the intraspecific slope, which may not always answer the biologically most meaningful questions. Moreover, its estimate of the intraspecific slope is biased when species are not independent of the predictor variable (Bafumi & Gelman, 2007). The within-species centring model we propose here (Eqn. 5; Notes S1) allows to separate trait relationships into within- and across-species components based on a standard LME syntax. As this model permits ‘borrowing strength’ (Tukey, 1972) across species via partial pooling (Gelman, 2006) to estimate an average within-species slope, it alleviates the issue of restricted trait ranges and small sample sizes within species, which, as mentioned earlier, can strongly affect the power of intraspecific analyses performed separately for each species.

## Conclusions

Our work provides clear evidence that across species, embolism resistance relates to both pit membrane thickness and vessel diameter, and that this diameter effect cannot be explained by an association of both diameter and embolism resistance with pit membrane thickness. Therefore, the  $D_h$ – $P_{50}$  relationship could either result from a functional link between  $D_h$  and  $A_p$ , or could be independent of  $A_p$ , driven for instance by multiphase processes at the gas–liquid–solid–surfactant interface in pit membranes, such as the dynamics of bubble behaviour. Future work should hence be directed at identifying the mechanisms that drive the  $D_h$ – $P_{50}$  relationship to reconcile recent models of embolism formation with anatomical evidence at the pit and vessel level, including vessel dimensions and connectivity. In this regard, both direct measurements of total intervessel pit area or number and mechanistic modelling of the processes behind embolism formation are crucial.

Furthermore, our study illustrates that inconsistencies in the  $D_h$ – $P_{50}$  relationship reported in the literature may be reinforced by differences in the size range of variables studied, missing covariates, and most importantly, the conflation of different scales of aggregation. The latter is underlined by the total absence of an intraspecific  $P_{50}$ – $D_h$  relationship, which contrasts with the pronounced interspecific trend in our dataset. The within-species centring model proposed expands the toolbox of trait-based ecology by a simple tool to separate cross-species and within-species patterns of trait associations.

## Acknowledgements

We thank the Bavarian State Institute for Viticulture and Horticulture, Veitshochheim, Germany, for granting us access to the Stutel-Arboretum facility, as well as Klaus Körber and all others involved in the 'Klimabäume Stutel' project. We thank Christine Gernert and Yvonne Heppenstiel, as well as all members of the Imaging Core Facility, University of Würzburg, for technical support. We further thank three anonymous reviewers for their valuable feedback. The Transmission Electron Microscope has been funded by the German Research Foundation (Deutsche Forschungsgemeinschaft DFG), grant no. 218894163. SJ and LK were financially supported by the German Research Foundation (DFG project no. 410768178). Open Access funding enabled and organized by Projekt DEAL.

## Competing interests








None declared.

## Author contributions

BS and JSC developed the original research questions, which were adjusted by EI and RML for the scope of the present study. FRT performed the measurements for the *A. monspessulanum* dataset. EI performed all other physiological and anatomical

measurements supported by LK and SJ, while RML performed the statistical analyses, and both prepared a first version of the manuscript, which was intensively discussed and revised by all authors. EI and RML share equal first authorship of this work. JSC and BS share equal senior authorship of this work.

## ORCID

Emilie Isasa  <https://orcid.org/0000-0002-5927-5151>  
 Steven Jansen  <https://orcid.org/0000-0002-4476-5334>  
 Lucian Kaack  <https://orcid.org/0000-0003-4705-2521>  
 Roman Mathias Link  <https://orcid.org/0000-0003-0588-3757>  
 Juliano Sarmiento Cabral  <https://orcid.org/0000-0002-0116-220X>  
 Bernhard Schuldt  <https://orcid.org/0000-0003-4738-5289>  
 Fon Robinson Tezeh  <https://orcid.org/0000-0002-6859-690X>

## Data availability

The dataset used for this study is available as a repository on data-dryad.org and can be accessed under the following doi: [10.5061/dryad.ns1rn8pxf](https://doi.org/10.5061/dryad.ns1rn8pxf).

## References

- Adams HD, Zeppel MJB, Anderegg WRL, Hartmann H, Landhäusser SM, Tissue DT, Huxman TE, Hudson PJ, Franz TE, Allen CD *et al.* 2017. A multi-species synthesis of physiological mechanisms in drought-induced tree mortality. *Nature Ecology & Evolution* 1: 1285–1291.
- Anderegg WRL, Klein T, Bartlett M, Sack L, Pellegrini AFA, Choat B, Jansen S. 2016. Meta-analysis reveals that hydraulic traits explain cross-species patterns of drought-induced tree mortality across the globe. *Proceedings of the National Academy of Sciences, USA* 113: 5024–5029.
- Anfodillo T, Olson ME. 2021. Tree mortality: testing the link between drought, embolism vulnerability, and xylem conduit diameter remains a priority. *Frontiers in Forests and Global Change* 4: 704670.
- Arend M, Link RM, Patthey R, Hoch G, Schuldt B, Kahmen A. 2021. Rapid hydraulic collapse as cause of drought-induced mortality in conifers. *Proceedings of the National Academy of Sciences, USA* 118: e2025251118.
- Bafumi J, Gelman A. 2007. Fitting multilevel models when predictors and group effects correlate. *SSRN Electronic Journal*. [WWW document] URL <https://ssrn.com/abstract=1010095> [accessed 8 May 2019].
- Bai H, Qian X, Fan J, Qian Y, Duo Y, Liu Y, Wang X. 2020. Computing pore size distribution in non-woven fibrous filter media. *Fibers and Polymers* 21: 196–203.
- Bland JM, Altman DG. 2011. Correlation in restricted ranges of data. *BMJ* 342: d556.
- Brodersen CR, McElrone AJ, Choat B, Lee EF, Shackel KA, Matthews MA. 2013. *In vivo* visualizations of drought-induced embolism spread in *Vitis vinifera*. *Plant Physiology* 161: 1820–1829.
- Bürkner P-C. 2017. BRMS: an R package for Bayesian multilevel models using Stan. *Journal of Statistical Software* 80: 1–28.
- Bürkner P-C. 2018. Advanced Bayesian multilevel modeling with the R package BRMS. *The R Journal* 10: 395–411.
- Champely S. 2020. *pwr: basic functions for power analysis*. [WWW document] URL <https://CRAN.R-project.org/package=pwr> [accessed 7 April 2022].
- Choat B, Badel E, Burlett R, Delzon S, Cochard H, Jansen S. 2016. Noninvasive measurement of vulnerability to drought-induced embolism by X-ray microtomography. *Plant Physiology* 170: 273–282.



- Choat B, Ball M, Luly J, Holtum J. 2003. Pit membrane porosity and water stress-induced cavitation in four co-existing dry rainforest tree species. *Plant Physiology* 131: 41–48.
- Choat B, Cobb AR, Jansen S. 2008. Structure and function of bordered pits: new discoveries and impacts on whole-plant hydraulic function. *New Phytologist* 177: 608–626.
- Christman MA, Sperry JS, Adler FR. 2009. Testing the ‘rare pit’ hypothesis for xylem cavitation resistance in three species of *Acer*. *New Phytologist* 182: 664–674.
- Clark JS, Bell DM, Hersh MH, Kwit MC, Moran E, Salk C, Stine A, Valle D, Zhu K. 2011. Individual-scale variation, species-scale differences: inference needed to understand diversity. *Ecology Letters* 14: 1273–1287.
- Cochard H, Damour G, Bodet C, Tharwat I, Poirier M, Améglio T. 2005. Evaluation of a new centrifuge technique for rapid generation of xylem vulnerability curves. *Physiologia Plantarum* 124: 410–418.
- Coles S, Bawa J, Trenner L, Dorazio P. 2001. *An introduction to statistical modeling of extreme values*. London, UK: Springer.
- Creek D, Blackman CJ, Brodribb TJ, Choat B, Tissue DT. 2018. Coordination between leaf, stem, and root hydraulics and gas exchange in three arid-zone angiosperms during severe drought and recovery. *Plant, Cell & Environment* 41: 2869–2881.
- Domec J-C, Schafer K, Oren R, Kim HS, McCarthy HR. 2010. Variable conductivity and embolism in roots and branches of four contrasting tree species and their impacts on whole-plant hydraulic performance under future atmospheric CO<sub>2</sub> concentration. *Tree Physiology* 30: 1001–1015.
- Fu P-L, Jiang Y-J, Wang A-Y, Brodribb TJ, Zhang J-L, Zhu S-D, Cao K-F. 2012. Stem hydraulic traits and leaf water-stress tolerance are co-ordinated with the leaf phenology of angiosperm trees in an Asian tropical dry karst forest. *Annals of Botany* 110: 189–199.
- Fuchs S, Leuschner C, Link RM, Schuldt B. 2021. Hydraulic variability of three temperate broadleaf tree species along a water availability gradient in central Europe. *New Phytologist* 231: 1387–1400.
- Gelman A. 2006. Multilevel (hierarchical) modeling: what it can and cannot do. *Technometrics* 48: 432–435.
- GIMP Development Team. 2018. *GIMP v.20.10.6*. [WWW document] URL <https://www.gimp.org/> [accessed 7 April 2022].
- Gleason SM, Westoby M, Jansen S, Choat B, Hacke UG, Pratt RB, Bhaskar R, Brodribb TJ, Bucci SJ, Cao K-F *et al.* 2016. Weak tradeoff between xylem safety and xylem-specific hydraulic efficiency across the world’s woody plant species. *New Phytologist* 209: 123–136.
- Grace JB, Schoolmaster DR, Guntenspergen GR, Little AM, Mitchell BR, Miller KM, Schweiger EW. 2012. Guidelines for a graph-theoretic implementation of structural equation modeling. *Ecosphere* 3: 1–44.
- Greenland S, Pearl J, Robins JM. 1999. Causal diagrams for epidemiologic research. *Epidemiology* 10: 37–48.
- Guan X, Pereira L, McAdam SAM, Cao K-F, Jansen S. 2021. No gas source, no problem: proximity to pre-existing embolism and segmentation affect embolism spreading in angiosperm xylem by gas diffusion. *Plant, Cell & Environment* 44: 1329–1345.
- Guan X, Werner J, Cao K-F, Pereira L, Kaack L, McAdam SAM, Jansen S. 2022. Stem and leaf xylem of angiosperm trees experiences minimal embolism in temperate forests during two consecutive summers with moderate drought. *Plant Biology* 24: 1208–1223.
- Hacke UG, Sperry JS, Wheeler JK, Castro L. 2006. Scaling of angiosperm xylem structure with safety and efficiency. *Tree Physiology* 26: 689–701.
- Hacke UG, Spicer R, Schreiber SG, Plavcová L. 2017. An ecophysiological and developmental perspective on variation in vessel diameter. *Plant, Cell & Environment* 40: 831–845.
- Hajek P, Kurjak D, von Wühlisch G, Delzon S, Schuldt B. 2016. Intraspecific variation in wood anatomical, hydraulic, and foliar traits in ten European beech provenances differing in growth yield. *Frontiers in Plant Science* 7: 791.
- Hajek P, Link RM, Nock CA, Bauhus J, Gebauer T, Gessler A, Kovach K, Messier C, Paquette A, Saurer M *et al.* 2022. Mutually inclusive mechanisms of drought-induced tree mortality. *Global Change Biology* 28: 3365–3378.
- Hargrave KR, Kolb KJ, Ewers FW, Davis SD. 1994. Conduit diameter and drought-induced embolism in *Salvia mellifera* Greene (Labiatae). *New Phytologist* 126: 695–705.
- Herbert E, Caupin F. 2005. The limit of metastability of water under tension: theories and experiments. *Journal of Physics: Condensed Matter* 17: S3597–S3602.
- Ingram S, Salmon Y, Lintunen A, Hölttä T, Vesala T, Vehkamäki H. 2021. Dynamic surface tension enhances the stability of nanobubbles in xylem sap. *Frontiers in Plant Science* 12: 732701.
- Jansen S, Choat B, Pletsers A. 2009. Morphological variation of intervessel pit membranes and implications to xylem function in angiosperms. *American Journal of Botany* 96: 409–419.
- Jansen S, Klepsch M, Li S, Kotowska MM, Schiele S, Zhang Y, Schenk HJ. 2018. Challenges in understanding air-seeding in angiosperm xylem. *Acta Horticulturae* 1222: 13–20.
- Johnson DM, Katul G, Domec J-C. 2022. Catastrophic hydraulic failure and tipping points in plants. *Plant, Cell & Environment* 45: 2231–2266.
- Kaack L, Altaner CM, Carmesin C, Diaz A, Holler M, Kranz C, Neusser G, Odstrcil M, Schenk HJ, Schmidt V *et al.* 2019. Function and three-dimensional structure of intervessel pit membranes in angiosperms: a review. *IAWA Journal* 40: 673–702.
- Kaack L, Weber M, Isasa E, Karimi Z, Li S, Pereira L, Trabi CL, Zhang Y, Schenk HJ, Schuldt B *et al.* 2021. Pore constrictions in intervessel pit membranes provide a mechanistic explanation for xylem embolism resistance in angiosperms. *New Phytologist* 230: 1829–1843.
- Kanduč M, Schneck E, Loche P, Jansen S, Schenk HJ, Netz RR. 2020. Cavitation in lipid bilayers poses strict negative pressure stability limit in biological liquids. *Proceedings of the National Academy of Sciences, USA* 117: 10733–10739.
- Klepsch M, Zhang Y, Kotowska MM, Lamarque LJ, Nolf M, Schuldt B, Torres-Ruiz JM, Qin D-W, Choat B, Delzon S *et al.* 2018. Is xylem of angiosperm leaves less resistant to embolism than branches? Insights from microCT, hydraulics, and anatomy. *Journal of Experimental Botany* 69: 5611–5623.
- Kotowska MM, Thom R, Zhang Y, Schenk HJ, Jansen S. 2020. Within-tree variability and sample storage effects of bordered pit membranes in xylem of *Acer pseudoplatanus*. *Trees* 34: 61–71.
- Lamarque LJ, Corso D, Torres-Ruiz JM, Badel E, Brodribb TJ, Burtlett R, Charrier G, Choat B, Cochard H, Gambetta GA *et al.* 2018. An inconvenient truth about xylem resistance to embolism in the model species for refilling *Laurus nobilis* L. *Annals of Forest Science* 75: 1–15.
- Lemaire C, Quilichini Y, Brunel-Michac N, Santini J, Berti L, Cartiailler J, Conchon P, Badel É, Herbette S. 2021. Plasticity of the xylem vulnerability to embolism in *Populus tremula* × *alba* relies on pit quantity properties rather than on pit structure. *Tree Physiology* 41: 1384–1399.
- Lemoine NP. 2019. Moving beyond noninformative priors: why and how to choose weakly informative priors in Bayesian analyses. *Oikos* 128: 912–928.
- Lens F, Gleason SM, Bortolami G, Brodersen C, Delzon S, Jansen S. 2022. Functional xylem characteristics associated with drought-induced embolism in angiosperms. *New Phytologist* 236: 2019–2036.
- Lens F, Sperry JS, Christman MA, Choat B, Rabae D, Jansen S. 2011. Testing hypotheses that link wood anatomy to cavitation resistance and hydraulic conductivity in the genus *Acer*. *New Phytologist* 190: 709–723.
- Lens F, Tixier A, Cochard H, Sperry JS, Jansen S, Herbette S. 2013. Embolism resistance as a key mechanism to understand adaptive plant strategies. *Current Opinion in Plant Biology* 16: 287–292.
- Levionnois S, Jansen S, Wandji RT, Beauchêne J, Ziegler C, Coste S, Stahl C, Delzon S, Authier L, Heuret P. 2021. Linking drought-induced xylem embolism resistance to wood anatomical traits in Neotropical trees. *New Phytologist* 229: 1453–1466.
- Levionnois S, Ziegler C, Jansen S, Calvet E, Coste S, Stahl C, Salmon C, Delzon S, Guichard C, Heuret P. 2020. Vulnerability and hydraulic segmentations at the stem–leaf transition: coordination across Neotropical trees. *New Phytologist* 228: 512–524.
- Li S, Lens F, Espino S, Karimi Z, Klepsch M, Schenk HJ, Schmitt M, Schuldt B, Jansen S. 2016. Intervessel pit membrane thickness as a key determinant of embolism resistance in angiosperm xylem. *IAWA Journal* 37: 152–171.
- Li S, Li X, Link RM, Li R, Deng L, Schuldt B, Jiang X, Zhao R, Zheng J, Li S *et al.* 2019. Influence of cambial age and axial height on the spatial patterns of xylem traits in *Catalpa bungei*, a ring-porous tree species native to China. *Forests* 10: 662.



- Loepfe L, Martinez-Vilalta J, Piñol J, Mencuccini M. 2007. The relevance of xylem network structure for plant hydraulic efficiency and safety. *Journal of Theoretical Biology* 247: 788–803.
- Losso A, Bär A, Dämon B, Dullin C, Ganthaler A, Petruzzellis F, Savi T, Tromba G, Nardini A, Mayr S *et al.* 2019. Insights from *in vivo* micro-CT analysis: testing the hydraulic vulnerability segmentation in *Acer pseudoplatanus* and *Fagus sylvatica* seedlings. *New Phytologist* 221: 1831–1842.
- Lübbe T, Lamarque LJ, Delzon S, Torres Ruiz JM, Burlett R, Leuschner C, Schuldt B. 2022. High variation in hydraulic efficiency but not xylem safety between roots and branches in four temperate broad-leaved tree species. *Functional Ecology* 36: 699–712.
- Maherali H, Moura CF, Caldeira MC, Willson CJ, Jackson RB. 2006. Functional coordination between leaf gas exchange and vulnerability to xylem cavitation in temperate forest trees. *Plant, Cell & Environment* 29: 571–583.
- Martínez-Vilalta J, Santiago LS, Poyatos R, Badiella L, Cáceres M, Aranda I, Delzon S, Vilagrosa A, Mencuccini M. 2021. Towards a statistically robust determination of minimum water potential and hydraulic risk in plants. *New Phytologist* 232: 404–417.
- Meyra AG, Kuz VA, Zarragoicoechea GJ. 2007. Geometrical and physicochemical considerations of the pit membrane in relation to air seeding: the pit membrane as a capillary valve. *Tree Physiology* 27: 1401–1405.
- Moles AT, Warton DI, Warman L, Swenson NG, Laffan SW, Zanne AE, Pitman A, Hemmings FA, Leishman MR. 2009. Global patterns in plant height. *Journal of Ecology* 97: 923–932.
- Mrad A, Domec J-C, Huang C-W, Lens F, Katul G. 2018. A network model links wood anatomy to xylem tissue hydraulic behaviour and vulnerability to cavitation: model links wood anatomy to plant hydraulics. *Plant, Cell & Environment* 41: 2718–2730.
- Mrad A, Sevanto S, Domec J-C, Liu Y, Nakad M, Katul G. 2019. A dynamic optimality principle for water use strategies explains isohydric to anisohydric plant responses to drought. *Frontiers in Forests and Global Change* 2: 49.
- Ogle K, Barber JJ, Willson C, Thompson B. 2009. Hierarchical statistical modeling of xylem vulnerability to cavitation. *New Phytologist* 182: 541–554.
- Olson ME, Anfodillo T, Rosell JA, Petit G, Crivellaro A, Isnard S, León-Gómez C, Alvarado-Cárdenas LO, Castorena M. 2014. Universal hydraulics of the flowering plants: vessel diameter scales with stem length across angiosperm lineages, habits and climates. *Ecology Letters* 17: 988–997.
- Paligi SS, Link RM, Isasa E, Bittencourt P, Cabral JS, Jansen S, Oliveira RS, Pereira L, Schuldt B. 2021. Accuracy of the pneumatic method for estimating xylem vulnerability to embolism in temperate diffuse-porous tree species (preprint). *bioRxiv*. doi: [10.1101/2021.02.15.431295](https://doi.org/10.1101/2021.02.15.431295).
- Pammenter NW, Vander Willigen C. 1998. A mathematical and statistical analysis of the curves illustrating vulnerability of xylem to cavitation. *Tree Physiology* 18: 589–593.
- Park J, Go T, Ryu J, Lee SJ. 2019. Air spreading through wetted cellulose membranes: Implications for the safety function of hydraulic valves in plants. *Physical Review E* 100: 32409.
- Pearl J. 2000. *Causality: models, reasoning, and inference*. Cambridge, UK: Cambridge University Press.
- Peel MC, Finlayson BL, McMahon TA. 2007. Updated world map of the Köppen-Geiger climate classification. *Hydrology and Earth System Sciences* 11: 1633–1644.
- Pfautsch S, Harbusch M, Wesolowski A, Smith R, Macfarlane C, Tjoelker MG, Reich PB, Adams MA. 2016. Climate determines vascular traits in the ecologically diverse genus *Eucalyptus*. *Ecology Letters* 19: 240–248.
- van de Pol M, Wright J. 2009. A simple method for distinguishing within- vs between-subject effects using mixed models. *Animal Behaviour* 77: 753–758.
- Pollet TV, Stulp G, Henzi SP, Barrett L. 2015. Taking the aggravation out of data aggregation: a conceptual guide to dealing with statistical issues related to the pooling of individual-level observational data: data aggregation and the ecological fallacy. *American Journal of Primatology* 77: 727–740.
- Poorter L, Castilho CV, Schiatti J, Oliveira RS, Costa FRC. 2018. Can traits predict individual growth performance? A test in a hyperdiverse tropical forest. *New Phytologist* 219: 109–121.
- Powers JS, Vargas GG, Brodribb TJ, Schwartz NB, Pérez-Aviles D, Smith-Martin CM, Becknell JM, Aureli F, Blanco R, Calderón-Morales E *et al.* 2020. A catastrophic tropical drought kills hydraulically vulnerable tree species. *Global Change Biology* 26: 3122–3133.
- Pratt RB, MacKinnon ED, Venturas MD, Crous CJ, Jacobsen AL. 2015. Root resistance to cavitation is accurately measured using a centrifuge technique. *Tree Physiology* 35: 185–196.
- R Core Team. 2022. *R: a language and environment for statistical computing*. Vienna, Austria: R Foundation for Statistical Computing. [WWW document] URL <https://www.R-project.org/> [accessed 5 November 2022].
- Reiss R-D, Thomas M. 2007. *Statistical analysis of extreme values: with applications to insurance, finance, hydrology and other fields*. Basel, Switzerland: Birkhäuser.
- Robinson WS. 1950. Ecological correlations and the behavior of individuals. *American Sociological Review* 15: 351–357.
- Rosell JA, Olson ME, Anfodillo T. 2017. Scaling of xylem vessel diameter with plant size: causes, predictions, and outstanding questions. *Current Forestry Reports* 3: 46–59.
- Roth-Nebelsick A. 2019. It's contagious: calculation and analysis of xylem vulnerability to embolism by a mechanistic approach based on epidemic modeling. *Trees* 33: 1519–1533.
- van der Sande MT, Poorter L, Schnitzer SA, Engelbrecht BMJ, Markesteijn L. 2019. The hydraulic efficiency–safety trade-off differs between lianas and trees. *Ecology* 100: e02666.
- Schenk HJ, Espino S, Romo DM, Nima N, Do AYT, Michaud JM, Papahadjopoulos-Sternberg B, Yang J, Zuo YY, Steppe K *et al.* 2017. Xylem surfactants introduce a new element to the cohesion-tension theory. *Plant Physiology* 173: 1177–1196.
- Schenk HJ, Espino S, Visser A, Esser BK. 2016. Dissolved atmospheric gas in xylem sap measured with membrane inlet mass spectrometry. *Plant, Cell & Environment* 39: 944–950.
- Schenk HJ, Steppe K, Jansen S. 2015. Nanobubbles: a new paradigm for air-seeding in xylem. *Trends in Plant Science* 20: 199–205.
- Schmid R, Machado RD. 1968. Pit membranes in hardwoods – fine structure and development. *Protoplasma* 66: 185–204.
- Schneider CA, Rasband WS, Eliceiri KW. 2012. NIH Image to IMAGEJ: 25 years of image analysis. *Nature Methods* 9: 671–675.
- Scholz A, Rabaey D, Stein A, Cochard H, Smets E, Jansen S. 2013. The evolution and function of vessel and pit characters with respect to cavitation resistance across 10 *Prunus* species. *Tree Physiology* 33: 684–694.
- Schuldt B, Knutzen F, Delzon S, Jansen S, Müller-Haubold H, Burlett R, Clough Y, Leuschner C. 2016. How adaptable is the hydraulic system of European beech in the face of climate change-related precipitation reduction? *New Phytologist* 210: 443–458.
- Shrier I, Platt RW. 2008. Reducing bias through directed acyclic graphs. *BMC Medical Research Methodology* 8: 70.
- Skelton RP, Anderegg LDL, Papper P, Reich E, Dawson TE, Kling M, Thompson SE, Diaz J, Ackerly DD. 2019. No local adaptation in leaf or stem xylem vulnerability to embolism, but consistent vulnerability segmentation in a North American oak. *New Phytologist* 223: 1296–1306.
- Skelton RP, Brodribb TJ, Choat B. 2017. Casting light on xylem vulnerability in an herbaceous species reveals a lack of segmentation. *New Phytologist* 214: 561–569.
- Sorek Y, Greenstein S, Netzer Y, Shtein I, Jansen S, Hochberg U. 2021. An increase in xylem embolism resistance of grapevine leaves during the growing season is coordinated with stomatal regulation, turgor loss point and intervessel pit membranes. *New Phytologist* 229: 1955–1969.
- Sperry JS, Nichols KL, Sullivan JEM, Eastlack SE. 1994. Xylem embolism in ring-porous, diffuse-porous, and coniferous trees of Northern Utah and Interior Alaska. *Ecology* 75: 1736–1752.
- Sperry JS, Tyree MT. 1988. Mechanism of water stress-induced xylem embolism. *Plant Physiology* 88: 581–587.
- Stroock AD, Pagay VV, Zwieniecki MA, Michele HN. 2014. The physicochemical hydrodynamics of vascular plants. *Annual Review of Fluid Mechanics* 46: 615–642.
- Subramanian SV, Jones K, Kaddour A, Krieger N. 2009. Revisiting robinson: the perils of individualistic and ecologic fallacy. *International Journal of Epidemiology* 38: 342–360.

- Torres-Ruiz JM, Jansen S, Choat B, McElrone AJ, Cochard H, Brodribb TJ, Badel E, Burtlett R, Bouche PS, Brodersen CR *et al.* 2015. Direct X-ray microtomography observation confirms the induction of embolism upon xylem cutting under tension. *Plant Physiology* 167: 40–43.
- Tukey JW. 1972. Data analysis, computation and mathematics. *Quarterly of Applied Mathematics* 30: 51–65.
- Tyree MT, Davis SD, Cochard H. 1994. Biophysical perspectives of xylem evolution: is there a tradeoff of hydraulic efficiency for vulnerability to dysfunction? *LAWA Journal* 15: 335–360.
- Tyree MT, Zimmermann MH. 2002. *Xylem structure and the ascent of sap*. Berlin & Heidelberg, Germany: Springer Verlag.
- Wason J, Bouda M, Lee EF, McElrone AJ, Phillips RJ, Shackel KA, Matthews MA, Brodersen C. 2021. Xylem network connectivity and embolism spread in grapevine (*Vitis vinifera* L.). *Plant Physiology* 186: 373–387.
- Wason JW, Anstreicher KS, Stephansky N, Huggett BA, Brodersen CR. 2018. Hydraulic safety margins and air-seeding thresholds in roots, trunks, branches and petioles of four northern hardwood trees. *New Phytologist* 219: 77–88.
- Weithmann G, Schuldt B, Link RM, Heil D, Hoeber S, John H, Müller-Haubold H, Schüller L-M, Schumann K, Leuschner C. 2021. Leaf trait modification in European beech trees in response to climatic and edaphic drought. *Plant Biology* 24: 1272–1286.
- Wheeler JK, Huggett BA, Tofte AN, Rockwell FE, Holbrook NM. 2013. Cutting xylem under tension or supersaturated with gas can generate PLC and the appearance of rapid recovery from embolism: sampling induced embolism. *Plant, Cell & Environment* 36: 1938–1949.
- Wheeler JK, Sperry JS, Hacke UG, Hoang N. 2005. Inter-vessel pitting and cavitation in woody Rosaceae and other vesselless plants: a basis for a safety vs efficiency trade-off in xylem transport. *Plant, Cell & Environment* 28: 800–812.
- White FM. 1991. *Viscous fluid flow*. New York, NY, USA: McGraw-Hill.
- Wickham H, Averick M, Bryan J, Chang W, McGowan LD, François R, Grolemund G, Hayes A, Henry L, Hester J *et al.* 2019. Welcome to the TIDYVERSE. *Journal of Open Source Software* 4: 1686.
- Yang J, Michaud JM, Jansen S, Schenk HJ, Zuo YY. 2020. Dynamic surface tension of xylem sap lipids. *Tree Physiology* 40: 433–444.
- Zhang Y, Carmesin C, Kaack L, Klepsch MM, Kotowska M, Matei T, Schenk HJ, Weber M, Walther P, Schmidt V *et al.* 2020. High porosity with tiny pore constrictions and unbending pathways characterize the 3D structure of intervessel pit membranes in angiosperm xylem. *Plant, Cell & Environment* 43: 116–130.
- Zhang Y, Klepsch M, Jansen S. 2017. Bordered pits in xylem of vesselless angiosperms and their possible misinterpretation as perforation plates. *Plant, Cell & Environment* 40: 2133–2146.
- Zimmermann J, Link RM, Hauck M, Leuschner C, Schuldt B. 2021. 60-year record of stem xylem anatomy and related hydraulic modification under increased summer drought in ring- and diffuse-porous temperate broad-leaved tree species. *Trees* 35: 919–937.

## Supporting Information

Additional Supporting Information may be found online in the Supporting Information section at the end of the article.

**Fig. S1** Raw data for the Cavitron vulnerability curves measured on the samples from the Stutel dataset.

**Fig. S2** Correlation matrix of the species level averages of the analysed variables.

**Notes S1** Fitting the within-species centring model with R.

**Table S1** Summary of the variables analysed.

**Table S2** Parameter estimates of the linear regression models.

**Table S3** Parameter estimates of the mixed-effects models.

Please note: Wiley is not responsible for the content or functionality of any Supporting Information supplied by the authors. Any queries (other than missing material) should be directed to the *New Phytologist* Central Office.